THE AMERICAN SOCIETY OF MECHANICAL ENGINEERS
345 E. 47th St., New York, N.Y. 10017

97-GT-474



# THE UNSTEADY PRESSURE FIELD OVER A TURBINE BLADE SURFACE: VISUALISATION AND INTERPRETATION OF EXPERIMENTAL DATA.


**Roger W Moss, Roger W Ainsworth, Colin D Sheldrake and Robert Miller**

Department of Engineering Science,
University of Oxford,
Parks Road,
Oxford, UK.
0044 1865 288754
roger.moss@eng.ox.ac.uk

## ABSTRACT

The unsteady static pressure field over a turbine rotor has been measured in the Oxford Rotor Facility using 78 flush-mounted miniature pressure transducers. This extensive surface coverage allows ensemble-averaged data to be displayed as an animated image. At the mid-height plane the fluctuations are well predicted using the UNSFLO 2-D unsteady code; away from mid-height the data shows large fluctuations.

12 transducers mounted on the blade leading edge show the relative total pressure field entering the blade row; these plus area traverse measurements at rotor exit are used to interpret the surface flow features. Rotor-mounted hot wires show large variations in blade incidence during the wake-passing cycle and allow conversion of blade-relative data into the absolute frame. Large pressure fluctuations in the root region may be explained in terms of a loss core associated with the NGV wake.

## NOMENCLATURE

| | |
|---|---|
| Cax | axial chord |
| Cv | specific heat at constant volume |
| NGV | nozzle guide vane |
| S | overall perimeter around blade surface |
| S | entropy |
| Tgrel | total temperature in blade-relative frame |
| Tw | blade metal temperature |
| U | velocity, m/s |
| x | axial distance from leading edge |
| X | perimeter from stagnation point to transducer |
| $\beta$ | flow angle in blade relative frame |
| $\delta_1$ | boundary layer momentum thickness |
| $\nu$ | kinematic viscosity |
| $\lambda$ | dimensionless acceleration parameter |

## INTRODUCTION

The demand for increased turbine efficiency, more accurate cooling design and greater accuracy in performance prediction leads to the consideration of time-unsteady CFD codes; despite the high time and hardware costs relative to time-steady calculations, unsteady solutions appear to be the most promising way of improving current design practice.

The use of such codes requires two levels of validation: one must both know which unsteady phenomena are worth studying as part of the design process and have confidence that the code delivers accurate predictions.

World-wide research using rotating turbine facilities started with studies into heat transfer phenomena (Ainsworth et al, 1988; Guenette et al, 1988; Dunn et al, 1988) and has since progressed to the study of aerodynamic phenomena.

Dring et al (1982) used a large scale, low speed, rotating facility to study rotor-stator interaction at two different axial spacings. 30 Kulite pressure transducers were used to measure blade and vane surface pressures together with 10 hot-film gauges to investigate the boundary layer state. Comparisons of suction and pressure surface data showed that the fluctuations were in phase across each passage i.e. on facing surfaces rather than on opposite sides of a single aerofoil. Large pressure fluctuations were observed on the suction side of the blade leading edge; these decayed towards the trailing edge. The decay rates showed the stator fluctuations to result purely

**Presented at the International Gas Turbine & Aeroengine Congress & Exhibition**
**Orlando, Florida — June 2–5, 1997**

from a potential flow interaction whereas the rotor experienced both wake and potential effects. The wake was seen to cause unsteady transition on the rotor suction surface.

Rai and Madavan (1990) used a 2-D unsteady Navier-Stokes code to perform a prediction based on the turbine tested by Dring (1982). Their time-mean pressure distribution was reasonably accurate; the predicted unsteady component was found to be dependent on the rotor/stator ratio which at the time could not be precisely modelled.

Korakianitis et al (1993) studied the mechanisms of unsteady heat transfer on a rotor blade using Unsflo and compared Unsflo heat transfer predictions against data from Calspan. No flow measurements were available, however, to confirm the accuracy of the flow prediction itself.

Kelecy et al (1995) performed a numerical study of the effect of vane-blade spacing on losses. They compared a 2-D unsteady prediction with blade mid-height data from Calspan and predicted peak-to-peak levels of pressure variation in reasonable agreement with the data.

Walraevens and Gallus (1995) used triple crossed hot wires and LDV to study the flow field and interactions in a stator-rotor-stator turbine facility. Vortices at each plane could be related to passage or trailing edge vortices from upstream blade rows. Zaccaria and Lakshminarayana (1995) used LDV to study the passage of NGV wakes through a rotor passage and the decay rate downstream.

Research at Oxford over the last ten years has concentrated on understanding unsteady physical phenomena and assessing their importance. Cascade testing by Doorly and Oldfield (1985) simulated wake and shock wave passing and showed that this led both to a characteristic AC shock signature, that could be predicted, and to boundary layer transition. The facility was subsequently converted to a rotating turbine from which a large amount of fast-response heat transfer and pressure data has been acquired (Dietz and Ainsworth 1992). Mid-height heat transfer and pressure data have been compared by Moss et al (1995). A 2-D unsteady prediction using Unsflo showed good predictions of surface pressure fluctuations and it was found that the heat transfer fluctuations could be usefully predicted from the isentropic temperature fluctuations associated with the measured pressures if one assumed a constant Nusselt number. This implied that wake-induced transition, as seen in cascade, was not a significant effect in the fully rotating facility: this is discussed further in Moss et al (1997). This paper describes further investigation of the flow-field based on static pressure data over the whole blade surface.

## INSTRUMENTATION

The Oxford Rotor is mounted in a transient flow turbine test facility based on an isentropic light piston tunnel (Ainsworth et al, 1988) that achieves engine representative Mach and Reynolds numbers (Table 1). The turbine is a transonic shroudless design of 0.5m tip diameter with a NGV-blade spacing of 0.346 NGV axial chords. Prior to a run the rotor is accelerated to 6000rpm, in vacuum, by an air motor. Compressed air drives a free-sliding piston down the pump tube (Figure 1), compressing the charge of air in front of it until a suitable pressure and temperature have been reached; a fast-acting annular valve then opens and the air passes through the turbine for 200ms. The turbine accelerates to 9500rpm and data is taken from the rotor instrumentation (via slip rings) for some 17 ms while it passes through the design condition. The data is captured on a 12-bit, 200kHz A-D system and processed subsequently using software running under Matlab. There are 36 nozzle guide vanes and 60 blades so the wake passing frequency (strictly speaking, the NGV passing frequency as seen in the blade-relative frame) is approximately 5 kHz. The 17 ms acquisition time is thus sufficient to capture 85 wake passing cycles.

The data presented here is assembled from over 400 signals captured during 120 tunnel runs and the run to run repeatability is sufficient to give a ±1.75% tolerance on $p/P_{rel}$ to a 95% confidence limit. This is equivalent to a Mach number accuracy of ±0.02 at a Mach number of 0.65.

Rotor instrumentation consists of sub-miniature Kulite pressure transducers (Ainsworth et al, 1990), thin-film heat transfer gauges (Ainsworth et al, 1989) with a 100kHz response and crossed hot wires (connected to an in-shaft anemometer, Sheldrake and Ainsworth 1995) projecting in front of the stagnation point at mid-height. The Kulite surface coverage is shown in Figure 2 and there are a total of 78 transducers. The leading edge transducers are mounted as pitots, with a bell-mouth projecting slightly in front of the leading edge; the others are embedded in the surface and sealed flush with a layer of silicone rubber. They cover an area of 1mm×1mm and have natural resonant frequencies of 500kHz so have sufficient resolution in both time and space to show shock and wake passing events in considerable detail. The transducers are arranged at spanwise positions of, nominally, 5, 10, 50, 90 and 95% of annulus height; these sections will be referred to as root, mid-root, mid-height, mid-tip and tip to facilitate description.

Signals from these transducers are ensemble averaged to remove random fluctuations and allow comparison of signals taken at similar locations but during different tunnel runs (Moss and Ainsworth, 1993). The ensemble averaging routine uses shaft position as determined using a pair of 1 and 36 line encoders; in practice, run to run variability led to the relative phase of all the signals being based on groups of signals that had been captured simultaneously, and absolute phase was set by comparison of a mid-height leading edge transducer with the Unsflo prediction.

| | |
|---|---|
| Rotor tip diameter | 554 mm |
| Blade axial chord | 24.35 mm |
| Design speed | 8434 rpm |
| Temperature ratio $T_{oin}/T_{s}$ | 1.138 |
| Blade Reynolds number $Re_{c_{ax}}$ | $1.554\times10^{6}$ |
| Blade exit Mn, isentropic. | 0.959 |

Table 1. Rotor nominal operating point.

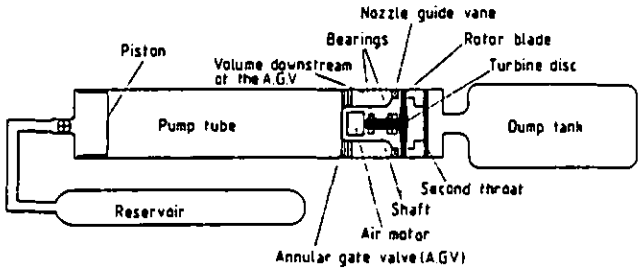


Figure 1. Layout of the Oxford Rotor transient test facility.

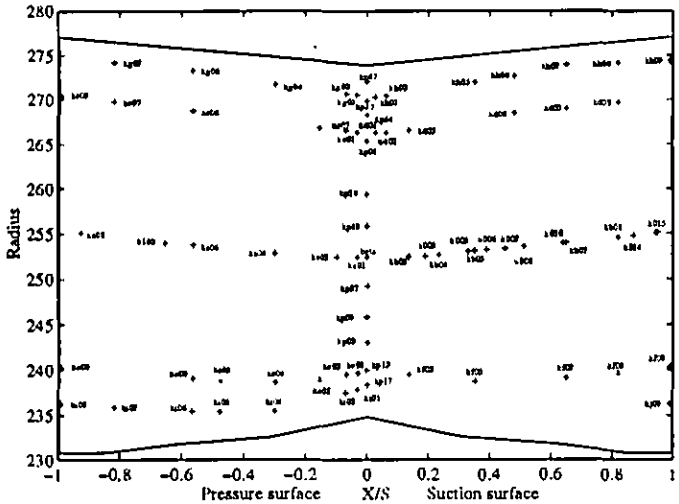


Figure 2. Kulite sensor positions on blade surface.

## CFD PREDICTIONS.

### Unsflo prediction details.

Unsflo is a 2-D viscous unsteady code written by Giles (1988) specifically for the prediction of stator-rotor interaction effects and uses Unsvis (a variant of Visual2) for its output processing. A grid resolution of 120x30 points was used for each stator passage (3 passages) plus 120x30 for each rotor passage (5 passages); the solution is briefly described by Ainsworth et al (1994). The Unsflo prediction is for the turbine mid-height plane; no attempt was made to run it for other spanwise sections because a 2-D code cannot be expected to produce realistic simulations in regions where the NGV exit flow must include significant radial velocity components due to secondary flow phenomena. A section of the grid is shown in Figure 3.

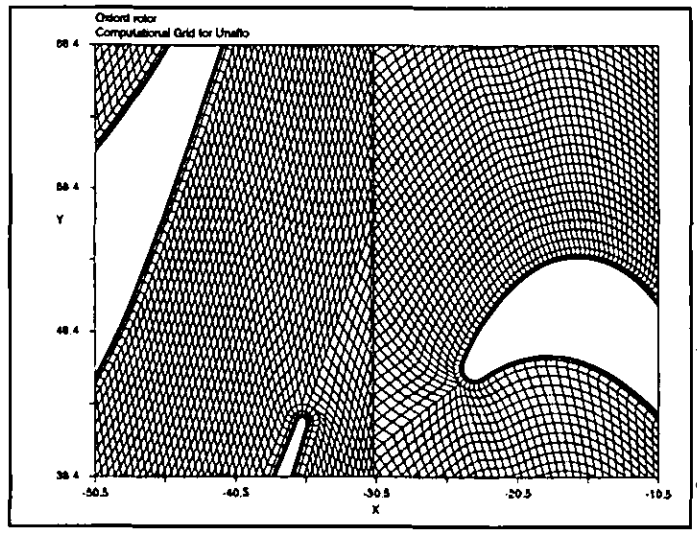


Figure 3. Part of the grid used for Unsflo predictions.

### Unsflo flow visualisation

The "Unsvis" output processor for Unsflo displays an animated sequence of colour contours for any flow parameter. Figure 4 shows the entropy prediction at six stages in the blade passing cycle. The nominal cycle positions refer to the blade in the centre of each image. The start of the "wake cycle" has been arbitrarily defined as the moment when a blade leading edge would intersect the path of an NGV wake in the absence of any wake distortion, i.e. if the wake were to continue in a straight line rather than wrapping around the blade aerofoil.

The entropy contours are useful in that they show the distortion of the NGV wake as it convects through the rotor and, in particular, the way that the wake wraps around the blade leading edge. The wake is in contact with the leading edge for a large part of the wake-passing period. This "wrap around" effect might be expected to result in the leading edge transducers not recording an obvious "wake signal" of the form that would be detected by a thin probe traversing through the NGV exit flowfield.

Figure 5 shows the equivalent blade-relative total pressure; the data is non-dimensionalised relative to the stage inlet conditions. When the blade reaches the 34% position it starts to interact with a region of high pressure just downstream of the NGV trailing edge. The effects from this will be discussed further in relation to the experimental data. The nominal NGV exit Mach number is 0.96 and so there might be a shock wave associated with this region; it is clear, however, from analysis at lower exit Mach numbers that this perturbed region persists even when a shock wave is not present.

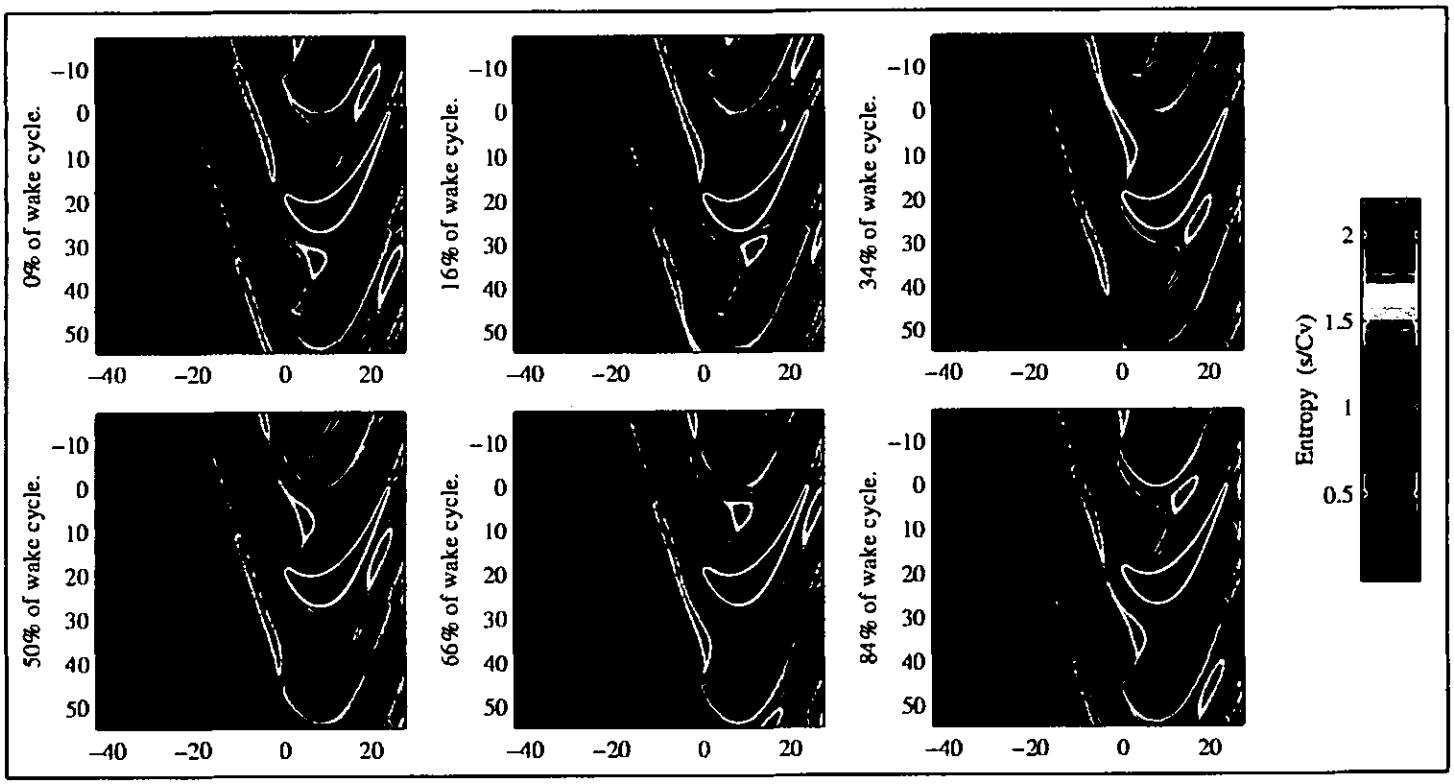


Figure 4. Unsflo entropy prediction: six stages in wake passing cycle.

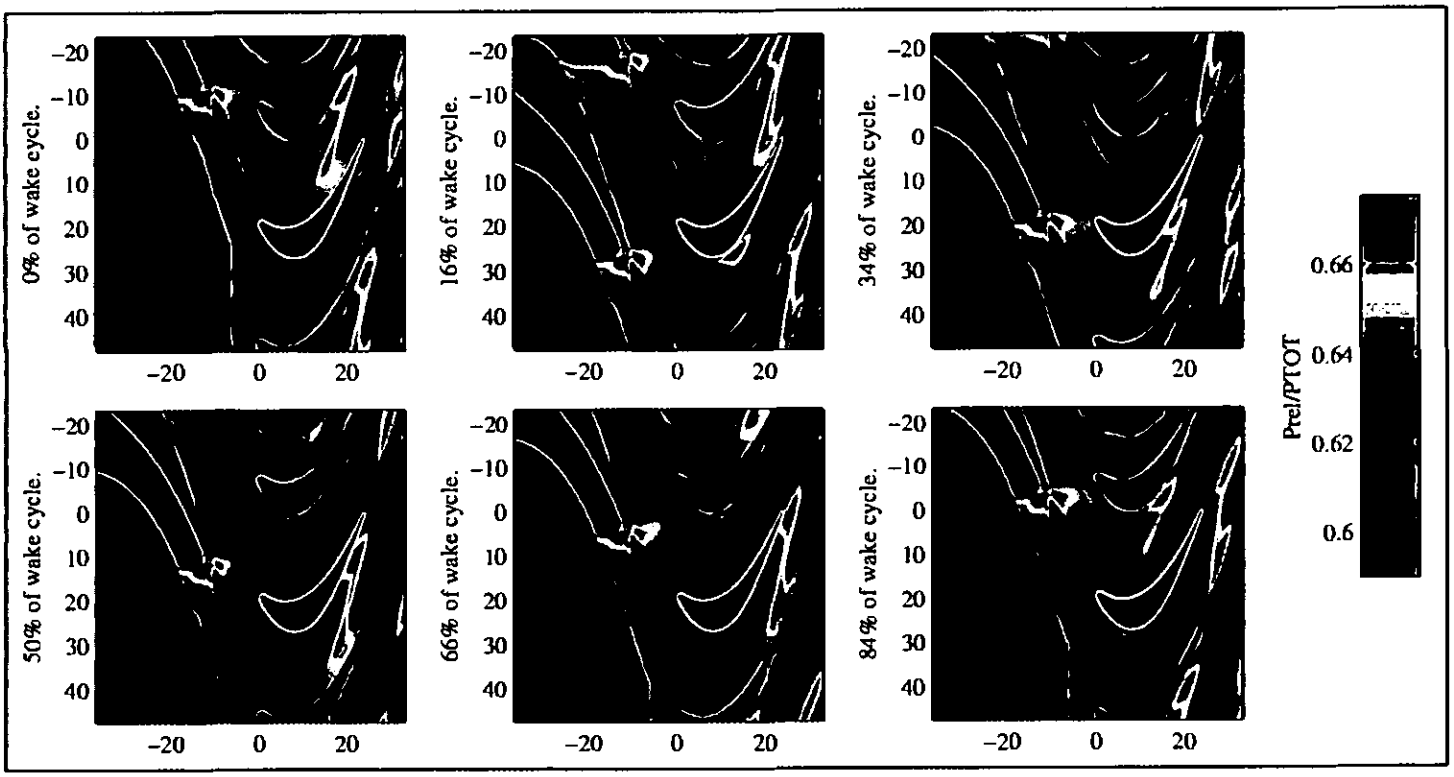


Figure 5. Unsflo total pressure prediction: six stages in wake passing cycle.

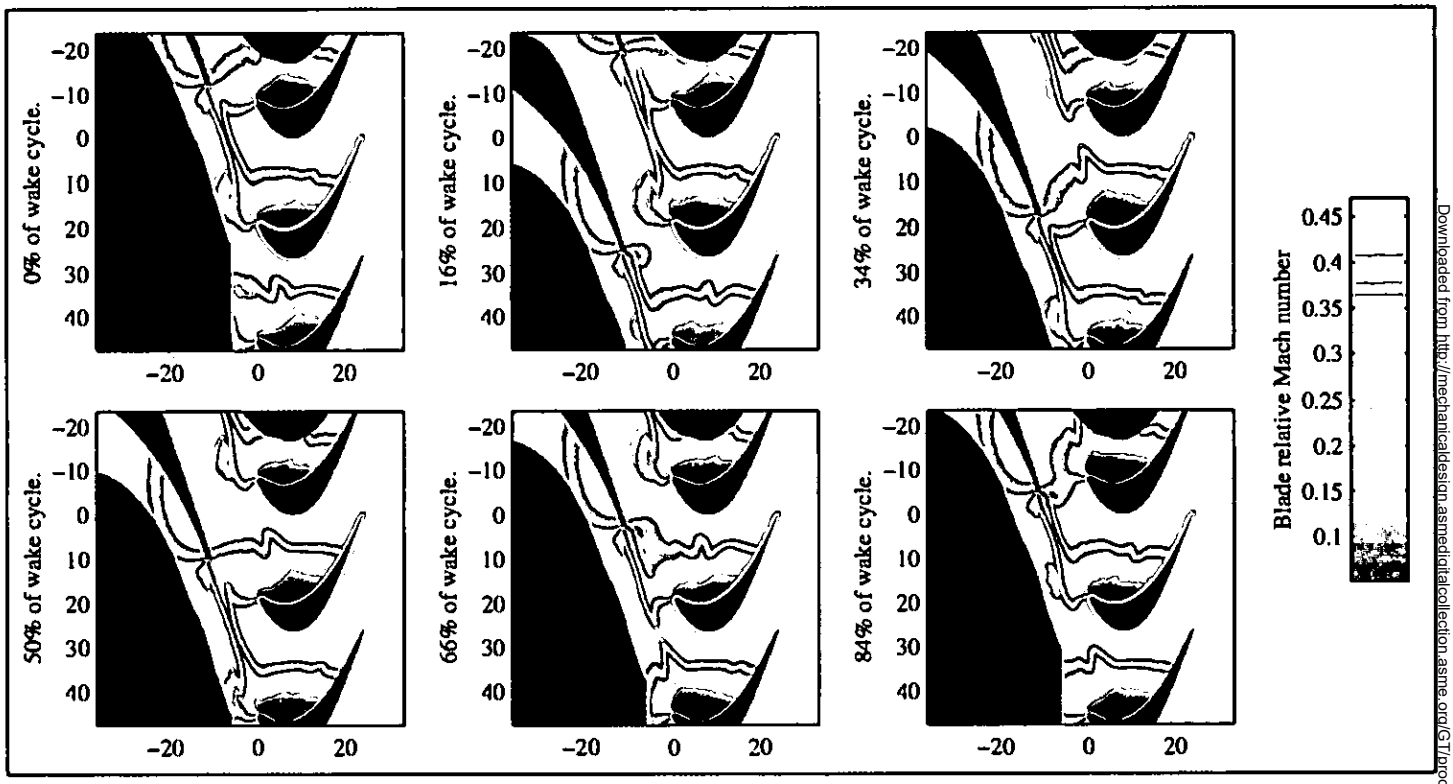


**Figure 6. Unsflo Mach number at six stages in wake passing cycle.**

Figure 6 shows the blade-relative Mach number. It is interesting to see the movement of the contours around the leading edge as the angle of incidence changes during the wake passing cycle. The hot wire mounted on the blade will inevitably be in a region of high Mach number gradient and thus very sensitive to such incidence changes. One can also see from the 34% image that, in addition to the blade leading edge entering the region of high static pressure described above, there is a change in the overall flow pattern as the wake from the previous NGV suddenly accelerates into the rotor passage and (in terms of velocity deficit) becomes rather less visible.

## Unsflo line probe results.

Unsvis allows one to draw a line across the display and see the instantaneous distribution of flow properties along it: this is known as a line probe. It has the further facility of then summing these instantaneous distributions throughout a blade cycle to produce the time-mean level at each point along the line.

Line probe data has been obtained along a line 2 mm axially in front of the blade leading edge plane: this represents the plane in which the leading edge hot wires and pitot kulites traverse.

Figure 7 show the line probe absolute total pressure results. The *x*-axes increase in the direction of blade movement i.e. pressure perturbations produced by the blades will move from left to right as time increases. The vertical grid lines show where wakes from the NGVs would intersect the line assuming a nominal wake angle of 69.16°. The thinner lines are instantaneous predictions for rotor disk positions denoted as *A*, *B* and *C* and the thicker line shows the time-mean prediction, averaged over a full blade-passing cycle, at each point. The instantaneous lines include points o+x to show points aligned with the blade leading edges further downstream at the same 69.16° angle. (The measured pressure could of course be derived from the locus of points o+x if one had a sufficient number of these traces). The blades corresponding to each of these points are each at a "wake cycle" position that can be inferred from the relative position of the NGV wake grid lines and the LE marker symbols; for instance, when the rotor is in position *A*, blade 1 is at 47% of a wake cycle, 2 is at 7% and 3 is at 67%. The line shown as "position *B*" occurs 20% of a cycle after *A*, and *C* occurs 20% after *B*.

One can see that the pressure measured by a Kulite at any point in the cycle is very different to the time-mean value at that point. This means that the pressures measured by blade leading edge transducers are unlikely to be explicable purely in terms of the time-mean NGV exit flow field and a velocity triangle calculation: the unsteady pressure is significantly influenced by the rotor-stator interaction.

Figure 8 shows the equivalent Mach number results. One can see from the slopes at the leading edge position markers that there is an appreciable Mach number gradient at these positions and that, as noted in the discussion of Figure 6, velocity measurements in this region will be very sensitive to the precise location of the probe.

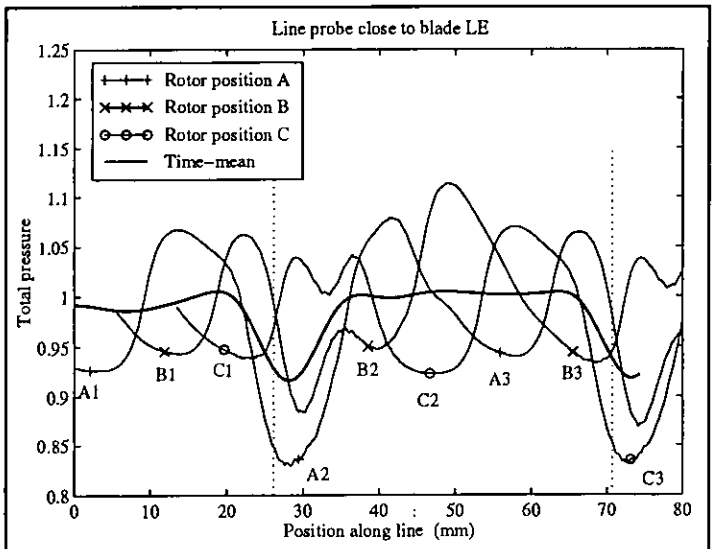


**Figure 7. Unsflo line probe prediction of absolute total pressure.**

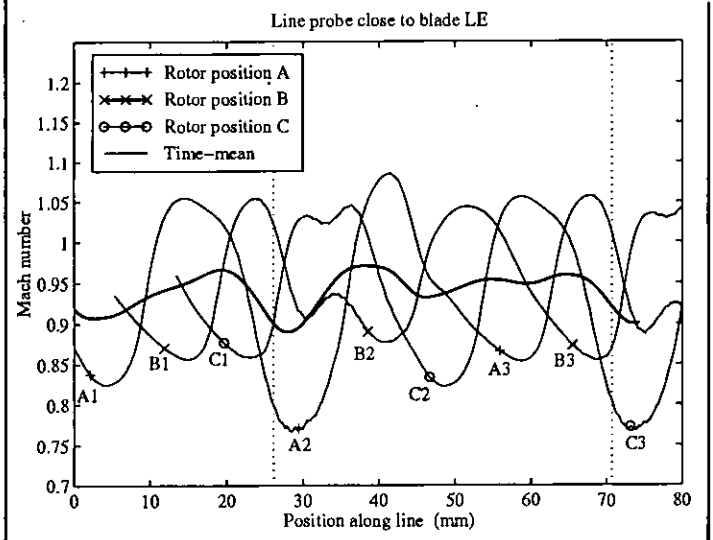


**Figure 8. Unsflo line probe prediction of absolute Mach number.**

## CFDS prediction details.

The Rolls-Royce CFDS 3-D steady viscous code (based on the Moore Elliptic Flow Program "MEFP", Moore, 1989) was run by Slater (1993) for this turbine geometry. CFDS is a three-dimensional viscous flow solver using a finite volume pressure prediction/correction algorithm and is designed specifically for the solution of turbomachinery flows. The measured NGV exit flowfield will be compared with Slater's CFDS prediction for the NGV using a 98x40x34 (133280 node) grid for the NGV, and time-mean blade surface pressures will be compared with a blade prediction using a 88x43x35 grid. These grids were the finest possible on the computers concerned. Previous calculations with coarser grids suggested that the grids were sufficiently fine to accurately predict surface pressure but possibly not fine enough for accurate heat transfer prediction through a turbulent boundary layer. Further details are given in Moss et al (1997).

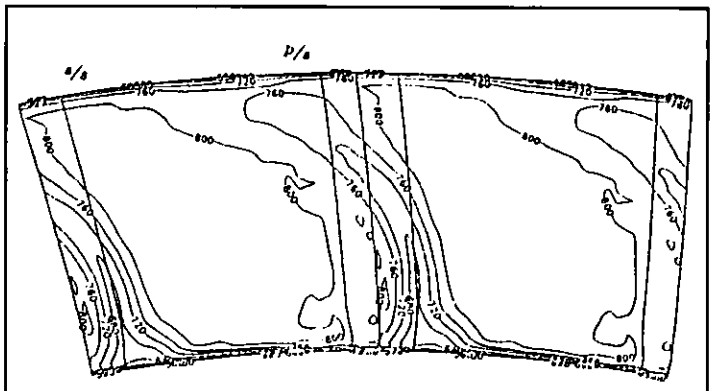

**Figure 9. CFDS NGV-only prediction of total pressure at rotor inlet plane.**

The CFDS prediction for this NGV at the rotor inlet plane (Figure 9) shows that the total pressure deficit in the wake increases from the tip to the root as the wake fluid migrates radially inwards. This CFDS calculation was for the nozzle guide vanes only i.e. no blades were present at the "rotor inlet plane". Close to the root, the wake also merges with the inner endwall secondary flow to create a deep loss core.

Figure 9 also shows that the predicted wake profile at the rotor inlet plane is inclined from the radial direction. The wake must have a purely radial orientation at the NGV exit plane because the NGV trailing edge is radially stacked (Figure 10). One can, however, also see from the stacking of the NGV aerofoils in Figure 10 that the exit angle increases towards the tip. This is shown more clearly in the CFDS exit angle prediction, Figure 11. The " $\tan(\alpha)/r$ = constant " line here shows the radial angle distribution that would be required to preserve the wake inclination as it moves towards the rotor if the NGV trailing edges lay in a single axial plane; in fact, the stator-rotor gap increases towards the tip and an alpha variation even smaller than that shown would preserve the radial wake alignment. CFDS predicts an exit angle variation much larger than the " $\tan(\alpha)/r$ = constant " line and so the wake will incline from the radial as it approaches the rotor inlet plane. The inclination seen in Figure 9 is thus not unexpected.

## COMPARISONS OF EXPERIMENTAL DATA WITH PREDICTIONS.

### Rotor leading edge Kulite data

The 12 leading edge pitot-mounted Kulites measure total pressure in the blade-relative frame and traverse the NGV exit flow field as they rotate through it. The blade mounted transducers are effectively, as discussed above, a rake probe with severe blockage - the measured pressures are influenced by the presence of the blade and will not be the same at each point as would be measured by an infinitely thin probe in the absence of any blade, nor will they equal the time-mean average values at this point.

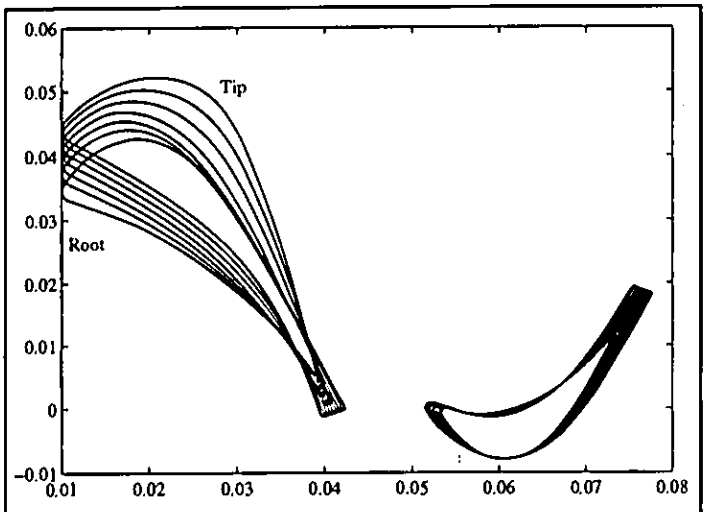


**Figure 10. View of NGV trailing edge and blade leading edge showing radial alignment.**

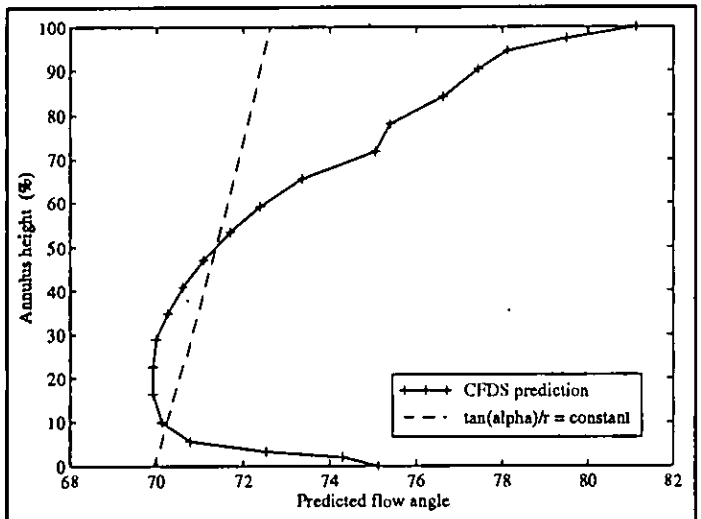


**Figure 11. Radial distribution of NGV exit angle as predicted by CFDS.**

The mean pressures measured by these leading edge Kulites are shown in Figure 12. The roll-off in blade-relative total pressure towards the blade root is to be expected from the high loss region that CFDS predicts at the root. The error bars indicate a 95% confidence limit based on the observed run to run scatter and number of available data points. The cause of the peaks and troughs in the data above a radius of 242 mm is unknown. It seems unlikely that there are errors of this size in the calibration coefficients and one must presume that at least part of this radial profile is a genuine product of the NGV exit flow field.

Figure 13 shows some typical data from leading edge Kulites at approximate radii, from the turbine centre line, of 238, 240, 246 and

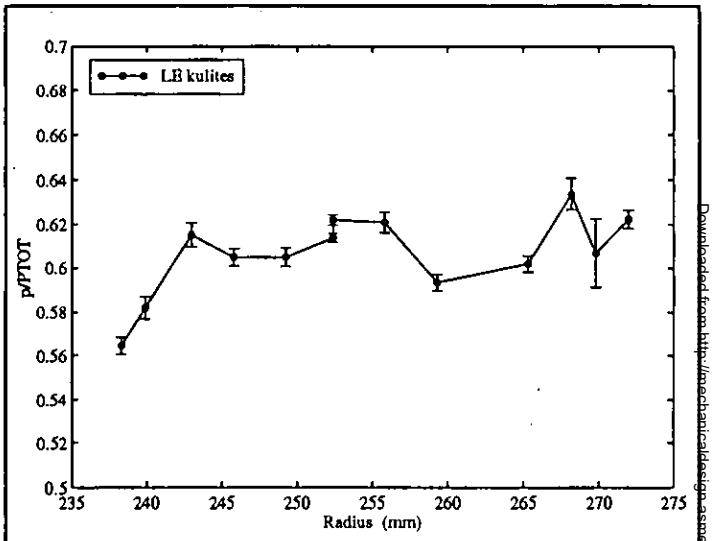


**Figure 12. Leading edge Kulites: time mean pressure levels.**

252 mm; these correspond to points 1, 2, 4 and 6 in Figure 12. The peak pressures from all the transducers are very similar but the two innermost transducers, kp17 and kp13, experience a much deeper wake than those closer to the blade mid-span. The increased wake strength at the root is responsible for the drop in mean level here.

It is interesting to note that Figure 13 shows considerable vane-to-vane variation in the depth of the wake. At present the causes of this are unknown: it is hoped that further investigation will enable it to be related to individual vane throat areas, trailing edge thicknesses or surface finish. All other data presented here has been ensemble averaged to remove this variability and enable "typical" wake passing features to be compared.

Cicatelli and Sieverding (1996) measured the spectrum resulting from vortex shedding in the wake of a large-scale nozzle guide vane. It is interesting to consider whether the present data would also show a spectral peak due to vortex shedding. They found vortices were shed with a Strouhal number of 0.27 which, at these conditions, would imply a frequency in the absolute frame of order 150kHz and a wavelength of 2.4 mm. The Doppler effect would reduce the apparent frequency in the relative frame to between 15 and 53 kHz, depending on the local velocity, and this should be easily detectable by the Kulites. There are, however, various reasons why such spectral peaks are unlikely to be seen in the current data.

The wake to wake variability will produce significant spectral noise at frequencies that are not harmonics of the wake passing frequency and this is likely to mask peaks due to vortex shedding. The ratio of wake length (NGV trailing edge to rotor inlet plane) to NGV trailing edge diameter is of order 50 and comparison with bar grid spectra (Moss and Oldfield, 1996) shows no evidence of peaks even at length:diameter ratios of only 8. Finally, one has to be sure that any spectral peaks are not a result of transducer resonance (Moss and Oldfield, 1991). Studies of the rotor Kulite spectra have so far failed to show any positively identifiable vortex shedding signature.

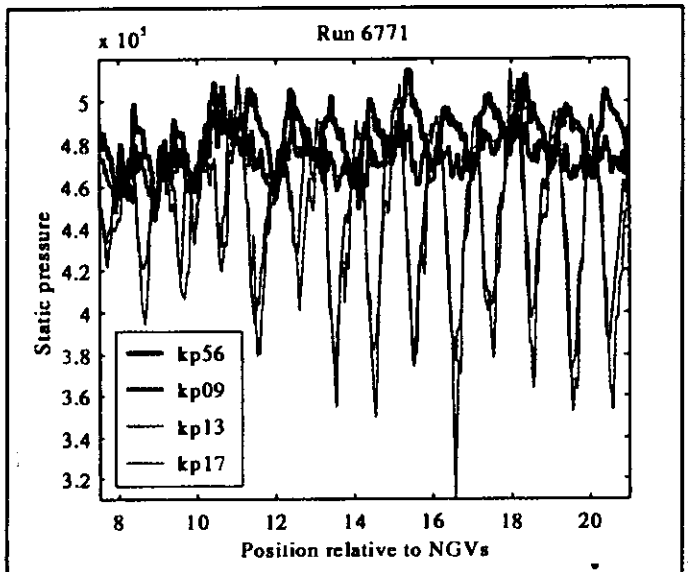


**Figure 13. Comparison of leading edge Kulite signals from transducers at radii of 238, 240, 246 and 252 mm.**

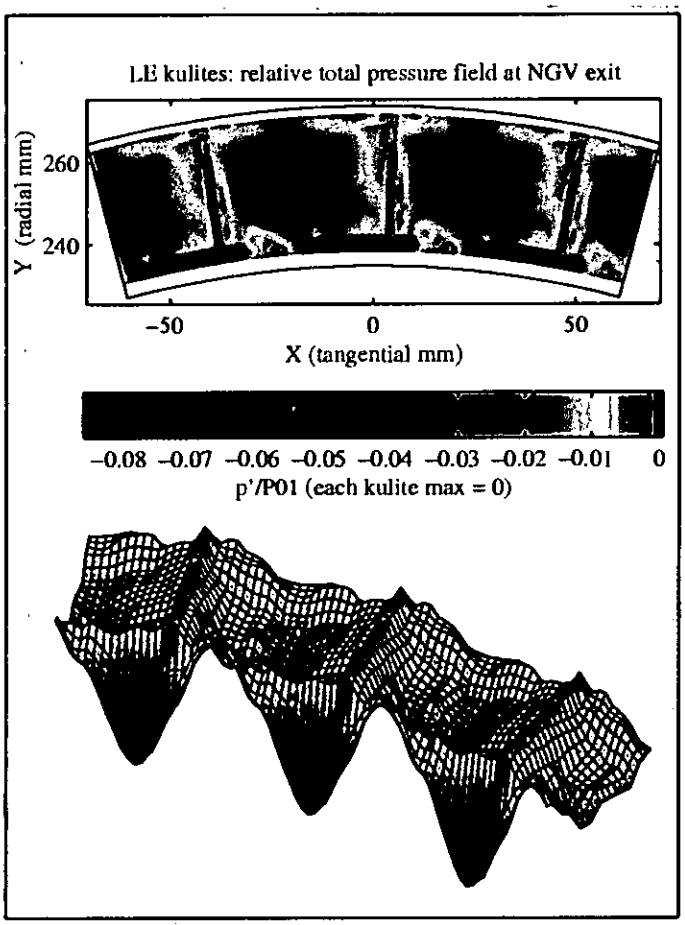


**Figure 14. NGV exit pressure field (relative frame) shifted to give each trace maximum = 0 and repeated over three passages.**

The large pressure deficit in the root region is clearly responsible for the size of the kp17 and kp13 wakes in Figure 13.

The NGV exit flow-field as measured by the passing of the blade leading edge Kulites is shown in Figure 14. The ensemble averaged data is plotted both as a contour plot and as a 3-D surface where the z-axis represents pressure. The NGV exit geometry is drawn as seen from downstream with the rotor rotating anticlockwise. The trace from each Kulite has been shifted in level such that its peak value is zero: this was done to eliminate the colour banding that would otherwise result from the unevenness in mean level seen in Figure 12. This shift in level is preferable to plotting the AC component because it preserves the appearance of the large wakes seen by the root transducers in Figure 13; it is also justified in that one expects the highest measured pressures to correspond to flow not subject to any losses, i.e. with absolute total pressure equal to that at stage inlet. Note that the gap between the root and mid-height peaks at 20% span in Figure 14 is purely an artefact of the plotting routine that fits a surface between the mid-passage ridge (Kulite kp02 and above) and the root peak (Kulites kp13 and kp17) which occurs about 1/5 of a cycle earlier.

The colour contours in Figure 14 show both wake features (blue) and a sharply defined mid-passage region of high relative total pressure (red). The wake appears to run almost radially, with the exception of the root region where a very large pressure deficit occurs some 40% of a cycle earlier that the mid-height wake. There is little sign of the inclination of the wake seen in the CFDS prediction. There is, as yet, no complete explanation for this discrepancy but it seems likely that it is a rotor-stator interaction effect. Figure 4 has shown that the wake wraps around the blade leading edge and does not move across it until some time after that which would be expected from purely geometrical considerations. The time at which the centre of the wake is detected by transducers at various spanwise positions may therefore be influenced by radial variations in the rotor lift coefficient.

The large periodic pressure deficits seen towards the root in Figure 14 must be caused by the deep loss core seen in Figure 9. The change in circumferential position relative to the CFDS prediction is unexpected; it may indicate an unsteady stator-rotor interaction, or an inability to accurately model a suitable NGV exit pressure distribution in the absence of the blade row. The CFDS grid upstream of the NGV was not as long as the full inlet duct in the experimental facility and so it is also possible that the endwall boundary layer thickness has been under predicted. This error is, however, unlikely to be large because the velocity in this inlet duct is low: the inlet boundary layer will reduce in thickness as it accelerates through the NGV and should make only a small contribution to the total boundary layer thickness at exit.

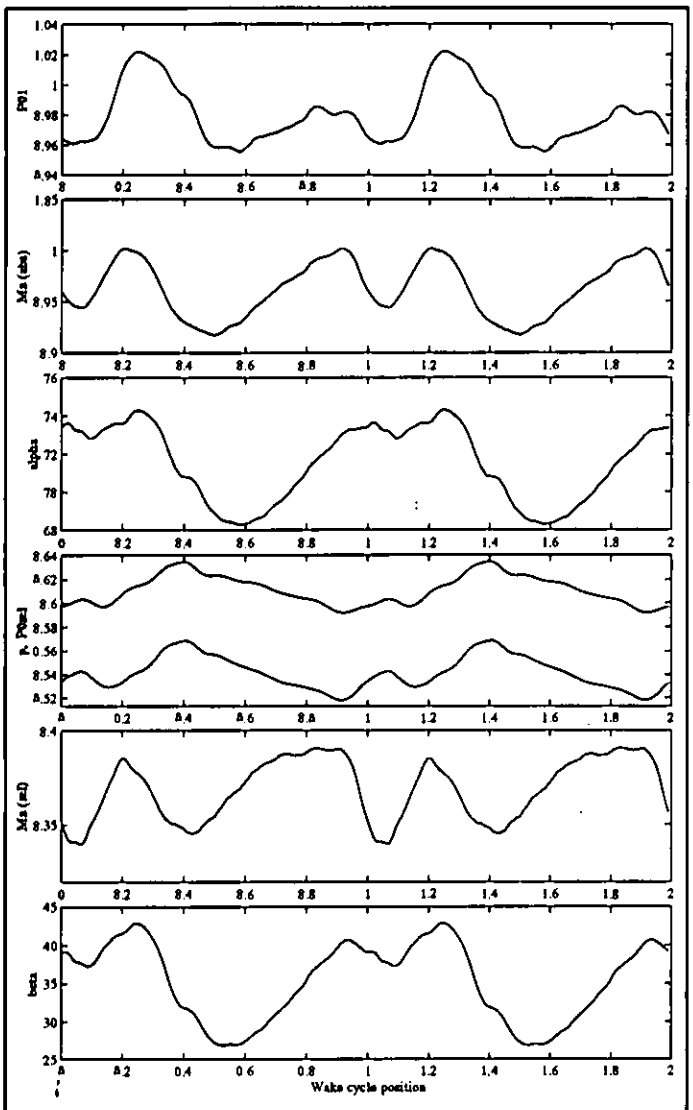


**Figure 15. Measured (blade-relative) and inferred (absolute) blade inlet conditions.**

The nature of the sharp mid-passage feature, shown red in Figure 14, may best be anderstood by converting the measurements into the absolute frame. This is possible at the mid-height section where crossed hot wires mounted on the rotor have provided relative Mach number and inlet angle data to complement the Kulite total pressure readings. This unsteady hot wire data has been shown to agree well (Moss et al, 1995) with the Unsflo prediction,, though there was some difference in time-mean levels which was attributed to difficulties in calibrating the wires over a very wide range of incidence. If one assumes a constant absolute total temperature (i.e. neglecting heat transfer to the vane, and assuming that the temperature effect of any stator-rotor interaction is small) one can calculate time histories for the static pressure, absolute total pressure and Mach number.

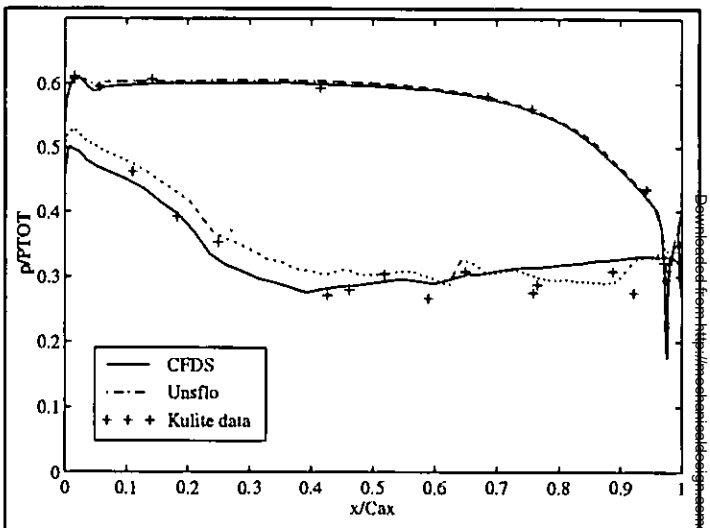


**Figure 16. Time-mean blade mid-height surface pressure distribution.**

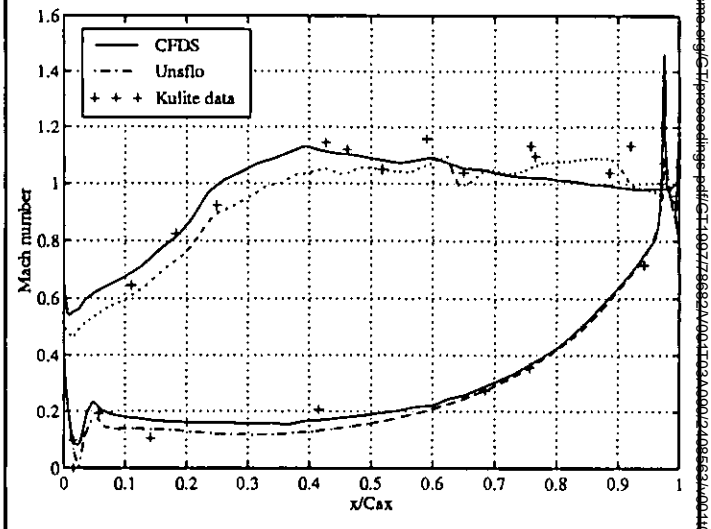


**Figure 17. Time-mean blade mid-height surface Mach number distribution corresponding to Figure 16 data.**

Two (repeated) cycles of the measured (blade-relative) and implied (absolute) pressures, angles and Mach numbers are shown in Figure 15. One can see that the peak in relative total pressure corresponds to a peak in static pressure as the Kulite moves into a high static pressure region located on the suction surface side of the NGV trailing edge. The sharpness of the change in pressure gradient suggests that there could be a weak shock wave here; such shocks have been seen in cascade Schlieren photographs.

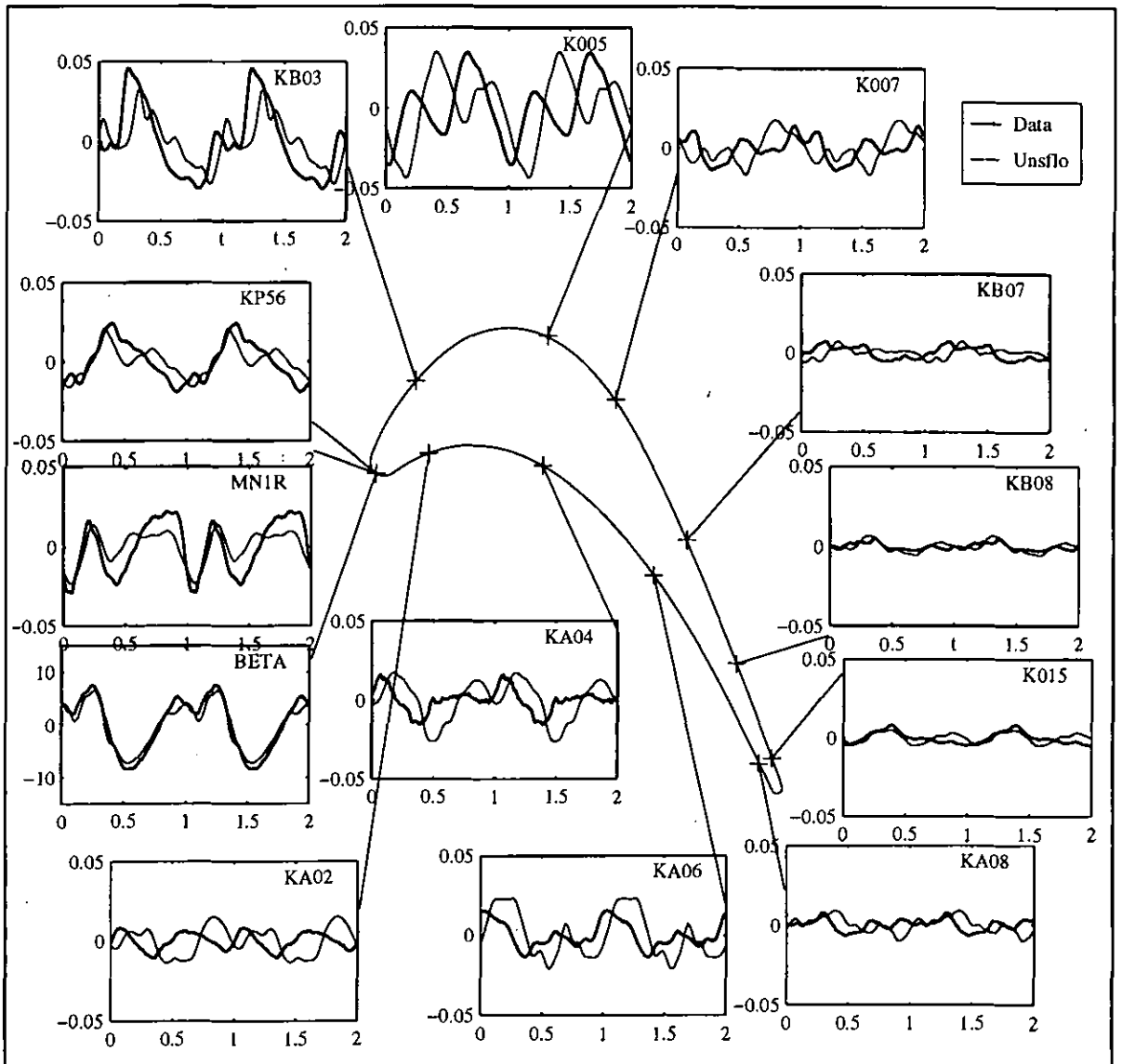


**Figure 18 AC component of mid-height Kulite data vs Unsflo prediction. Phase of data has been set to align with Unsflo at the leading edge.**

## Blade mid-height static pressure data

Figure 16 compares the mid-height data with CFDS and Unsflo predictions. The data agrees quite reasonably with both CFDS and Unsflo though it appears that the exit pressure used for CFDS may be slightly too high.

The data used in Figure 16 has been converted to Mach number and is shown in Figure 17. The experimental Mach number distributions are calculated from the local time-mean static pressures and the blade-relative mean total pressures at the leading edge (as shown in Figure 12). Viscous codes such as MEFP and Unsflo do not, strictly speaking, calculate surface Mach numbers since the no-slip condition at the surface implies zero velocity. These "Mach numbers" are included here simply to illustrate the transonic nature of this turbine. The flow close to the rear suction surface has a Mach number of approximately 1.1 and will thus be very sensitive to small variations in surface curvature. The authors believe that the fluctuations in Mach number and pressure seen on the late suction surface accurately reflect the pressure distribution on this aerofoil rather than resulting from calibration errors.

The AC component of the Unsflo surface pressure prediction is compared with data from the mid-height Kulites in Figure 18. Crossed hot wire blade-relative measurements of Mach number and yaw angle at the leading edge are also included as `mn1r` and `beta`. The data agrees well with the prediction at the leading edge. In general one can see that Unsflo has predicted the correct rms fluctuation level at most positions. The predictions on the pressure surface and the suction surface crown are, however, out of phase

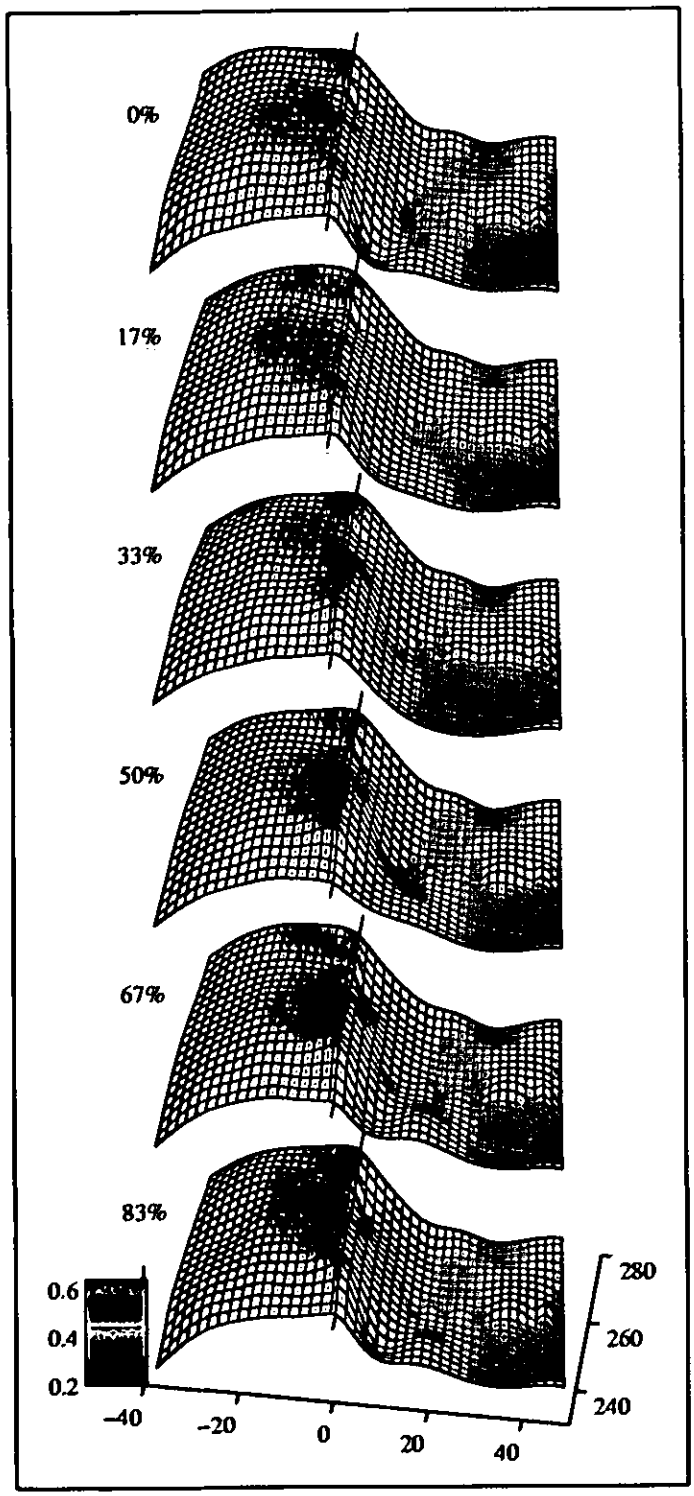


**Figure 19. Blade surface pressure: 6 stages in wake passing cycle.**

relative to the measurements and the predicted waveform differs from that measured. The largest pressure fluctuations are found on the suction surface crown rather that at the leading edge. This contrasts with previous research (Dring et al. 1982) in a low Mach number facility which found the largest fluctuations close to the leading edge.

## Static pressure data over whole blade surface

Static pressure data from all 78 Kulites has been interpolated onto a uniform grid covering the blade surface to allow instantaneous values to be plotted as a 3-D surface of pressure against blade surface length and radial position. The interpolated data is plotted in Figure 19 at six stages in the wake passing cycle. The percentage cycle position is shown to the left of each surface.

All data are plotted against developed surface length from the nominal (mean camber line) stagnation point; the pressure surface is designated as having a negative surface length. Pressure data is normalised relative to the absolute total pressure at stage inlet. The upturned corner of the surface at the suction surface trailing edge (root) is the result of a single Kulite on this streamline and as such cannot be discussed with great confidence.

The lines protruding from each surface at x=0 in Figure 19 show the mean camber line leading edge position and one can see that the stagnation point is very close to this in the root region, though at mid-height and above the stagnation point appears to move slightly onto the pressure surface.

The level of pressure fluctuation is generally small, the exception being at the mid-root on the suction surface crown where one can see a large fluctuation - compare, for instance, the results for cycle positions of 33% and 67%.

These fluctuations at the mid-root section appear as an elevated pressure on Kulite kf05 at the 67% cycle position and produce a severely distorted pressure distribution (Figure 20); this cannot easily be converted to instantaneous Mach number as the total pressure at each Kulite position cannot be measured. One can see from the β plot in Figure 15 that at this instant the blade experiences nearly 15° negative incidence relative to the nominal 42° relative inlet angle; this incidence change, together with the highly perturbed inlet flow seen in Figure 14, appears to be the main cause of the peak. One might suspect that the adverse pressure gradient at this moment would cause separation. The laminar acceleration parameter $\lambda = \frac{\frac{dU}{dx}\delta_2^2}{\nu}$ is plotted in Figure 21 and reaches a minimum of -4.5: in the steady state, if the boundary layer was laminar, separation would be inevitable. The momentum thickness Reynolds number is, however, estimated as 3014 based on the time-mean Nusselt number so the boundary layer must be turbulent.

Heat transfer measurements from a thin film gauge close to the kf05 Kulite position (Figure 22) show that for most of the wake passing cycle the unsteady signal can be closely predicted from the

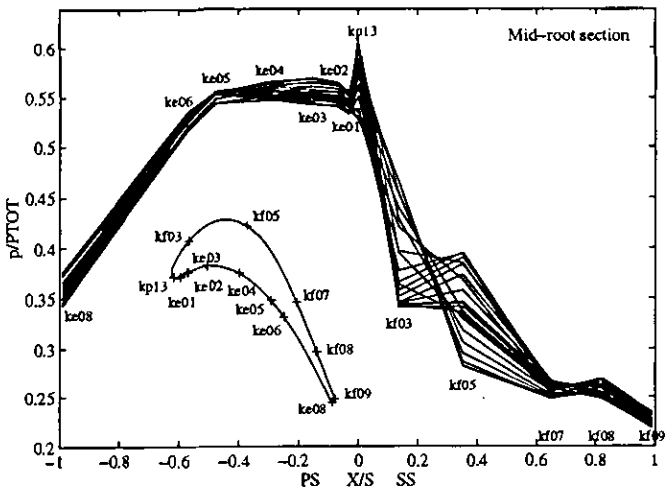


Figure 20. Unsteady pressure distribution at mid-root section.

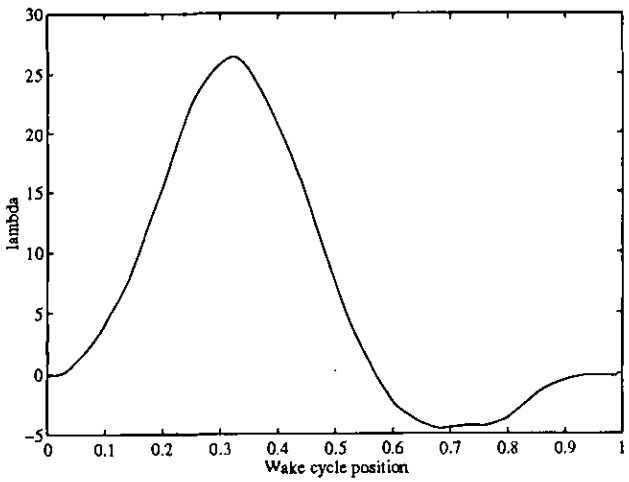


Figure 21. Acceleration parameter between kf03 and kf05 positions.

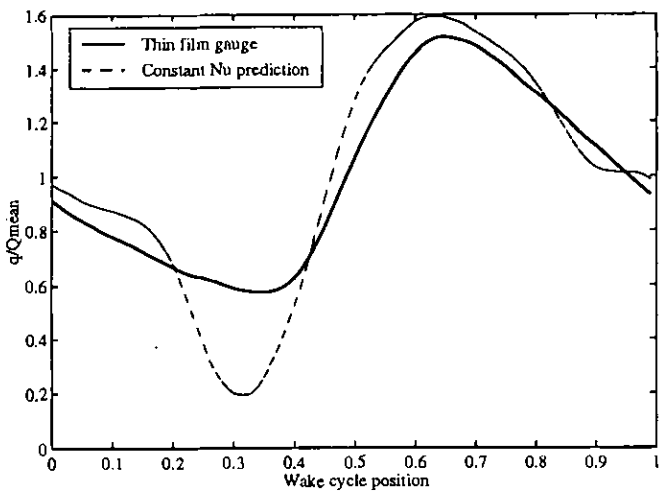


Figure 22. Measured and predicted heat flux at kf05 position.

isentropic temperature fluctuations by assuming a constant Nusselt number (as Moss et al, 1995). The measured pressure reaches a minimum around the 33% cycle position and the discrepancy between the measured heat flux and the prediction at this point suggests that the relative total temperature must rise above the mean level at this instant. The excellent agreement over the rest of the cycle indicates that unsteady separation or relaminarisation is not occurring. One may deduce the large pressure fluctuations arise from the blade pressure distributions with a non-uniform inlet flow at extreme incidence angles rather than from an unsteady separation.

## Space-Time diagrams of fluctuations along a streamline.

Pressure fluctuations over the blade surface are very easily seen on a computer generated animation of a surface similar to those seen in Figure 19. A printed sequence of "snapshots" as shown here is less easy to interpret and small fluctuations may escape notice. Figure 23 shows space-time diagrams for four of the instrumented sections (10%, 50%, 90%, 95% span) and has been included for the benefit of readers who might otherwise have difficulty in assessing the presence or amplitude of fluctuations in regions of interest.

The inclined lines on the space-time diagrams indicate propagation at Mach 1: any feature that is "flatter" than this will appear to be travelling faster than Mach 1 and vice-versa. The colours indicate the instantaneous pressure at each gauge position relative to the mean level there; as before, the pressure is normalised relative to stage inlet total. The red points along the upper edge of the graph indicate the Kulite positions.

The mid-root section shows that the large disturbance seen on the suction surface crown appears first at the leading edge and then propagates rearwards at a Mach number of approximately 0.5.

Both the mid-height and mid-tip sections show some features moving forwards on the early suction surface; and the mid-tip and tip sections also show a forwards moving feature on the rear pressure surface. Close examination of the Unsflo animations shows that such features are actually predicted; the wake touches the pressure surface near the trailing edge shortly before it hits the rest of the late pressure surface. Schlieren photographs of this aerofoil in cascade (Johnson et al, 1988) provide further insight: shock waves from a moving bar wake generator hit the suction surface crown before moving forwards towards the leading edge.

## CONCLUSIONS

The combination of unsteady pressure and heat transfer data from the blade surface with unsteady CFD predictions both gives credence to the CFD capabilities and assists in the interpretation of the data.

At mid-height, flow fluctuations seen at the leading edge result from the blade passing through a high static pressure region that occurs on the suction surface side of the NGV trailing edge. Contour plots at

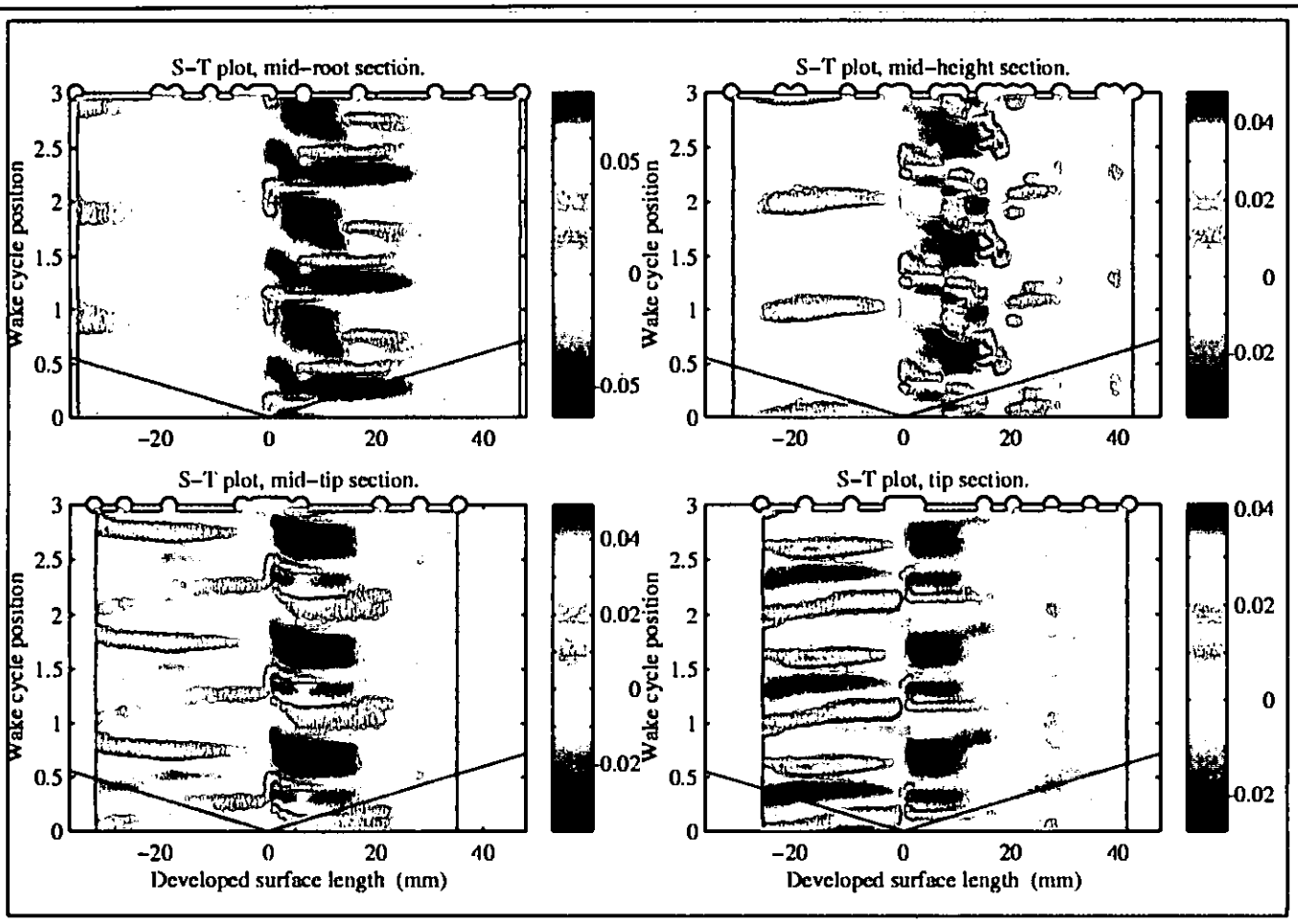


**Figure 23. Space/cycle phase diagram of pressure fluctuations along instrumented streamlines.**

various stages through the cycle, and line probe data, show that the observed pressure fluctuations are significantly influenced by the presence of the blade and could not be accurately predicted by velocity triangle calculations based on the time-mean NGV exit flow.

The agreement between the unsteady pressure data and Unsflo predictions is very close in the leading edge region. Further downstream Unsflo predicts appropriate rms levels but there are discrepancies in phase and waveform. Time-mean surface pressures from Unsflo are close to the observed distribution.

The NGV exit pressure field shows wakes and a mid-passage low Mach number region that are more nearly radial than predicted by a time-steady 3-D calculation for the NGV. It appears that vane-blade interactions may influence the time at which such features interact with the blade leading edge. Very large pressure fluctuations are seen towards the root where NGV wake fluid migrates to form a loss core.

Large static pressure fluctuations are seen on the blade at 10% span around the crown of the suction surface. These are associated with the loss core at the root and the severe negative incidence that it causes. Heat transfer data indicate that the boundary layer here must be predominantly turbulent and this conclusion is reinforced by the apparent absence of any separation despite a strong adverse pressure gradient. The investigation of such regions via 3-D unsteady design codes should be seen as an essential part of the design process. The quality of 2-D unsteady predictions from Unsflo suggests that current 3-D codes should give useful results in this respect.

The data presented here is believed to be unique in terms of its high frequency response, extensive surface coverage, achievement of realistic Mach and Reynolds numbers and agreement with prediction.

A programme of 3-D unsteady Navier-Stokes predictions for this turbine stage is currently in progress and will be the subject of a future paper.

## ACKNOWLEDGEMENTS

The authors would like to thank Rolls-Royce plc, the Defence Research Agency (Pyestock), the Ministry of Defence and the Department of Trade and Industry for their support of this work.

## REFERENCES

Ainsworth, R.W., Schultz, D.L., Davies, M.R.D., Forth, C.J.P., Hilditch, M.A., Oldfield, M.L.G. and Sheard, A.G., 1988, "A Transient Flow Facility for the Study of the Thermofluid Dynamics of a Full Stage Turbine Under Engine Representative Conditions", ASME 88-GT-144

Ainsworth, R.W., Allen, J.L., Davies, M.R.D., Doorly, J.E., Forth, C.J.P., Hilditch, M.A., Oldfield, M.L.G. and Sheard, A.G., 1989, "Developments in Instrumentation and Processing for Transient Heat Transfer Measurements in a Full Stage Model Turbine", ASME Journal of Turbomachinery, Vol 111, January 1989, pp20-27.

Ainsworth, R.W. Dietz, A.J., and Nunn, T.A., 1990, "The Use of Semi-Conductor Sensors for Blade Surface Pressure Measurement in a Model Turbine Stage". ASME 90-GT-346

Ainsworth, R.W., Allen, J.L., and Batt, J.J.M., 1994, "The Development of Fast Response Aerodynamic Probes for Flow Measurements in Turbomachinery", ASME 94-GT-23.

Cicatelli, G. and Sieverding, C.H., 1996, "The Effect of Vortex Shedding on the Unsteady Pressure Distribution around the Trailing Edge of a Turbine Blade", ASME 96-GT-359

Dietz, A.J., and Ainsworth, R.W., 1992, "Unsteady Pressure Measurements on the Rotor of a Model Turbine Stage in a Transient Flow Facility", ASME 92-GT-156

Doorly, D.J. and Oldfield, M.L.G., 1985, "Simulation of Wake Passing in a Stationary Turbine Rotor Cascade", AIAA Journal of Propulsion and Power, Vol. 1, No. 4, p316.

Dring, R.P., Joslyn, H.D., Hardin, L.W. and Wagner, J.H., 1982, "Turbine Rotor-Stator Interaction", ASME Journal of Engineering for Power, October 1982, Vol 104, pp 729-742.

Dunn, M.G., Seymour, P.J., Woodward, S.H., George, W.K., and Chupp, R.E., 1988, "Phase-Resolved Heat Transfer Measurements on the Blade of a Full-Scale Rotating Turbine", ASME 88-GT-173

Giles, M.B., 1988, "Calculation of Unsteady Wake-Rotor Interaction", AIAA Journal of Propulsion and Power, Vol. 4, pp356-362.

Guenette, G.R., Epstein, A.H., Giles, M.B., Haimes, R., and Norton, R.J.G., 1988, "Fully Scaled Transonic Turbine Rotor Heat Transfer Measurements". ASME 88-GT-171

Johnson, A.B., Rigby, M.J., Oldfield, M.L.G., Ainsworth, R.W. and Oliver, M.J., 1988, "Surface Heat Transfer Fluctuations on a Turbine Rotor Blade Due To Upstream Shock Wave Passing". ASME 88-GT-172

Kelecy, F.J., Griffin, J.W., and Delaney, R.A., 1995, "The Effect of Vane-Blade Spacing on Transonic Turbine Stage Performance", AGARD CP571, "Loss Mechanisms and Unsteady Flow in Turbomachines", Paper 5.

Korakianitis, T., Papagiannidis, P, and Vlachopoulos, N.E., 1993, "Unsteady-Flow/Quasi-Steady Computations on a Turbine Rotor and Comparison with Experiments". ASME 93-GT-145

Moss, R.W. and Ainsworth, R.W., 1993, "A Transient Measuring Technique for Heat Transfer to Metallic Aerofoils". Proc. Eurotherm 32, Heat Transfer in Single Phase Flows, Oxford.

Moss, R.W. and Oldfield, M.L.G, 1991, "Measurements of Hot Combustor Turbulence Spectra", ASME 91-GT-351

Moss, R.W. and Oldfield, M.L.G, 1996, "Effect of Free-Stream Turbulence on Flat Plate Heat Flux Signals: Spectra and Eddy Transport Velocities", ASME Journal of Turbomachinery, July 1996, Vol 118 No. 3 pp. 461 - 467 (also 94-GT-205)

Moss, R.W., Sheldrake, C.D., Ainsworth, R.W., Smith, A.D., and Dancer, S.N., 1995, "Unsteady Pressure and Heat Transfer Measurements on a Rotating Blade Surface in a Transient Flow Facility", AGARD CP571, "Loss Mechanisms and Unsteady Flow in Turbomachines", Paper 22.

Moss, R.W., Ainsworth, R.W., and Garside, T., 1997, "Effects Of Rotation On Blade Surface Heat Transfer: An Experimental Investigation", To be presented at ASME Turbo Expo, Florida, 1997

Rai, M.M. and Madavan, N.K., 1990, "Multi-Aerofoil Navier-Stokes Simulations of Turbine Rotor-Stator Interaction", ASME Journal of Turbomachinery, July 1990, Vol 112, pp 377-384.

Sheldrake, C.D., and Ainsworth, R.W., 1995, "The Use of Hot-Wires Applied to Aerodynamic Measurements in a Model Turbine Stage", First European Conference on Turbomachinery Fluid Dynamic and Thermodynamic Aspects, Nuremberg.

Slater, J.T., 1993, "Three-Dimensional Aerodynamic Studies of a Turbine Stage in a Transient Flow Facility". DPhil Thesis, University of Oxford.

Walraevens, R.E., and Gallus, H.E, 1995, "Stator-Rotor-Stator Interaction in an Axial Flow Turbine and its Influence on Loss Mechanisms", AGARD CP571, "Loss Mechanisms and Unsteady Flow in Turbomachines", Paper 39.

Zaccaria, M.A., and Lakshminarayana, B., 1995, "Unsteady Flow Field Due To Nozzle Wake Interaction With The Rotor In An Axial Flow Turbine: Part 1 - Rotor Passage Flow Field", ASME 95-GT-295.